2024 IEEE/RSJ International Conference on Intelligent Robots and Systems (IROS)
October 14-18, 2024. Abu Dhabi, UAE

Pseudo-Domain Adversarial Networks with Electrical Impedance Tomography for Electrode Offset Error

Gengchen Xu[1,2], Haofeng Chen[1,2], Xuanxuan Yang[1,2], Gang Ma[*2], Xiaojie Wang[*1]

Abstract— **This paper propose a novel transfer learning approach, Pseudo-Domain Adversarial Network (PDAN), to tackle the issue of electrode displacement in Electrical Impedance Tomography (EIT). Electrode displacement, caused by human movement or improper operation, significantly affects the accuracy of EIT by introducing data errors. Existing solutions either modify the electrode assembly at a high cost or employ recognition algorithms that require retraining from scratch. To overcome these limitations, our work leverages the power of transfer learning to enhance model performance in the target domain by utilizing knowledge from a related task in the source domain. PDAN extends the capabilities of deep adversarial learning by incorporating noisy images to simulate post-electrode rotation scenarios, aiding in the reduction of negative impacts caused by minor electrode displacements. Our method demonstrates superior performance in classifying leg posture data, achieving around 90% accuracy, and proving robust against sensor electrode offset. Experimental results across various datasets validate the effectiveness of PDAN, indicating its potential in addressing complex real-world situations with improved generalization capabilities.**

I. Introduction

Electrical Impedance Tomography (EIT) is a non-invasive imaging technique that measures the interior structural impedance distribution of a conductive object [1]. Due to the non-destructive of EIT, it has also been applied in the medical field, such as neonatal skull imaging [2] and cancer detection [3]. It has also been utilized in human-computer interaction [4], such as equipment for leg health recognition [5] and detection of a sensor-integrated soft robot [6]. However, during the process of collecting impedance data by EIT, electrodes may experience displacement [7] [8] as the human body moves to cause data errors, making it challenging to continue using models trained previously. The electrode displacement can eventually result in serious consequences such as difficulties in system calibration and data distortion. Recognizing the significance of addressing this issue, researchers have explored various solutions, ranging from physical modifications to algorithmic approaches.

Olmos et al. [9] proposed physical modifications to electrode arrangements and control systems to mitigate displacement-related challenges. However, this method entails high hardware costs, limiting its scalability. On the other hand, Kunori et al. attempted to insert electrodes directly into the organism [10], directly exploring the activity state of the rat's cerebral cortex under different conditions using cortical stimulation and optical imaging. Although this operation does not require high costs, prolonged puncturing can damage the organism. Electrodes in this state do not possess long-term stability and biological compatibility.

While changing the electrode assembly method at the physical level resolves the electrode displacement phenomenon, it introduces issues of high cost or harm to the human body. Therefore, some individuals approach the problem from the perspective of recognition algorithms. For example, using the mathematical method of Non-negative Matrix Factorization (NMF) [11] to decompose high-frequency temporal features obtained before and after electrode rotation, excluding interference factors, and evaluating the effect through classification. Another approach involves establishing a set of suitable filters, such as Common Spatial Patterns (CSP) [12], to recognize signals before and after rotation. Alternatively, Shi et al. [13] established a prior relationship matrix for conditions before and after electrode offset, reducing its impact by modifying the matrix. These studies directly address the electrode displacement problem by focusing on temporal feature changes in signals generated by electrode movement [11] [12]. These techniques aim to address signal changes induced by electrode movement but require frequent retraining, posing resource consumption challenges and limiting their practicality.

To overcome the limitations of existing solutions, we propose using transfer learning. Transfer learning improves performance on a related task (target domain) by leveraging knowledge learned on another task (source domain). It involves applying models and knowledge trained on large datasets to accelerate learning on new tasks. Transfer learning typically involves applying pre-trained base models to new tasks. They are trained on large-scale datasets and have proven to learn more general features, avoiding the resource consumption associated with retraining [14] [15]. Meanwhile, by fine-tuning the final and label layers of the network in transfer learning, preliminary results show an improvement in classification accuracy after electrode displacement. However, this has only been demonstrated in theoretical models with two electrodes [16]. Furthermore, in previous research, Tammina et al. [17] explored and compared three methods: not using transfer learning, using only data augmentation, and combining transfer learning with data

[1]Gengchen Xu, Haofeng Chen, Xuanxuan Yang and Xiaojie Wang are with the Institute of Intelligent Machines, Hefei Institutes of Physical Science, Chinese Academy of Sciences, Hefei 230031, China.

[2]Gengchen Xu, Haofeng Chen, Xuanxuan Yang and Gang Ma are with the University of Science and Technology of China, Hefei, Anhui 230026, China.

This work was supported in part by the National Natural Science Foundation of China (Grant NO.62303436); in part by National Key R&D Program of China (2023YFB4704600in part by the Fundamental Research Funds for the Central Universities under Grant WK5290000004

[*]Corresponding author: Gang Ma (e-mail: magang93@ustc.edu.cn) Xiaojie Wang (e-mail: xjwang@iamt.ac.cn)

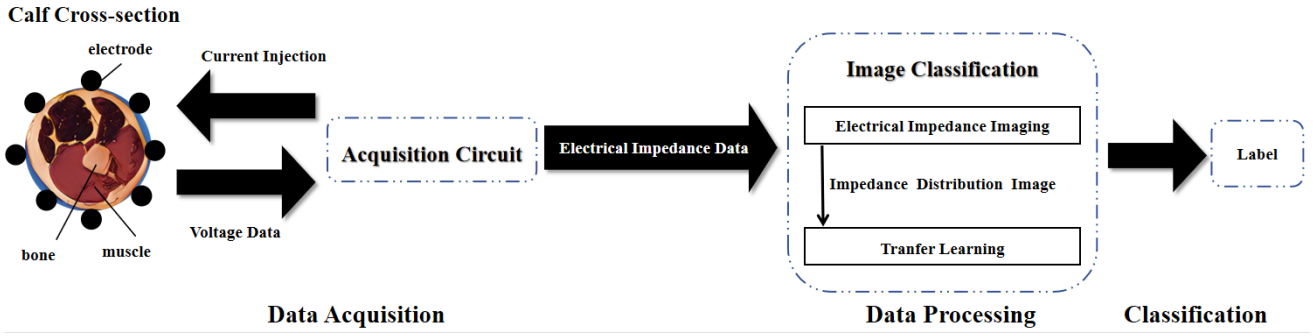

Fig. 1. The overall process of using transfer learning to process leg electrical impedance imaging. In the first stage, collect data. The second stage involves electrical impedance imaging and classification.

augmentation. The strategy of combining transfer learning achieved the best results, demonstrating the effectiveness of transfer learning.

Therefore, this paper proposes a new transfer learning method called Pseudo-Domain Adversarial Networ (PDAN) to address the issue of electrode displacement in complex real-world situations. In real-world scenarios, models trained with simple transfer learning often experience a decline in generalization performance on the target domain [18], while PDAN significantly extends the capabilities of deep adversarial learning. By incorporating noisy images to simulate real-world scenarios, PDAN improves model robustness, ensuring reliable performance even in the presence of electrode displacement. During the training process of the model to recognize real and noisy images, this helps alleviate the negative impact transmission caused by minor electrode displacement in the actual end-to-end framework training process. Model evaluations based on the accuracy of classifying the dataset and real-time classification results demonstrate the effectiveness of PDAN in real-time classification tasks, highlighting its practical utility in dynamic environments.

The organization of the article is as follows. In Section 2, we mainly focus on the main components of the entire system. We describe the process of conducting experiments to validate the leg posture classification model, analyzing the classification results and possible causes in Section 3. Finally, in Section 4, we discuss our findings and summarized our work.

II. System Design

The entire EIT system architecture is shown in Fig.1. It comprises three parts: data acquisition, data processing and classification. Firstly, the impedance data of human tissues is determined by homemade data acquisition system. The leftmost part of the figure is the cross-section of the human calf, mainly composed of muscles and bones. The black part represents the electrode, which is attached to the surface of the human body. Next, the acquisition circuit applies current to the human calf to obtain the returned voltage data. The data is transformed into impedance distribution images through EIT. Finally, the image results are sent to a laptop for training and recognition through transfer learning. The returned label is the type of leg posture we predicted.

A. Data Acquisition

In Figure 2, we present the acquisition system consisting of an AD5940 chip and ECG electrodes. Alcohol is first applied to the calves of the human body to remove dust and impurities to prevent further impact on data collection. Then the electrodes are evenly attached to the calf of the subject and connected to the acquisition chip through a crocodile clip. The acquisition chip is designed utilizing an AD5940 Impedance Analyzer as its foundation. This chip includes a frequency generator and an on-board ADC enabling impedance measurement within a specific frequency range from 0 Hz to 100 KHz with a resolution of 0.1 Hz.

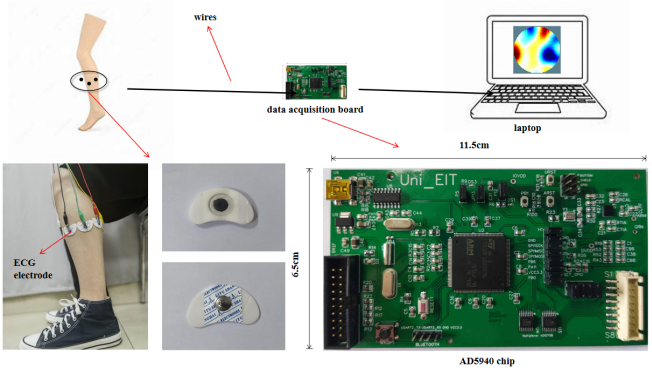

Fig. 2. The acquisition system includes the AD5940 chip and ECG electrodes. The electrodes are tightly attached to the surface of the human calf, and the extended wires are connected to the AD55940 chip.

We collect voltage data in a two-terminal scheme with 8 electrodes. Its working principle involves utilizing a pair of electrodes for impedance measurement. In this system, only two electrodes are employed for both current injection and voltage measurements. The impedances between all electrodes pairs were measured sequentially without repetition, which resulted in 28 independent values. We opt for the two-terminal scheme primarily because it necessitates fewer electrodes for impedance measurement, thereby reducing hardware complexity.

The medical electrode consists of a conductive silicone layer and other auxiliary layers. The silver layer ensures the transmission of current, while the auxiliary layer ensures intimate contact between the electrodes and the human body. To differentiate between various gestures, it is imperative that the surface electrodes are firmly attached to the skin, ensuring consistent and stable contact impedance between the electrodes and the skin throughout each test. Hence, we opt for commercial medical electrodes that have a track record of use in electromyography (EMG) signal measurement.

B. Data Processing

The imaging process of EIT involves forward and inverse problems. The forward problem of EIT refers to the situation where the conductivity distribution σ of the measured field and the excitation signal are known, and the boundary potential U of the field is solved.

$$U = F(\sigma) \tag{1}$$

To save computational resources, we simplify the physical model of EIT for the leg as follows: the conductivity of the human body is isotropic and does not change with the strength of the electric field. Therefore, we employ the finite element method for solving, linearizing the problem leads to Equation (1) transformed into

$$\delta U = \boldsymbol{J}\delta\sigma \tag{2}$$

where $\boldsymbol{J} \in R^{m\times n}$ is the sensitivity matrix, $\delta U \in R^m$ is the boundary voltages change, $\delta\sigma \in R^n$ is the conductivity change. The ultimate goal is to solve for the distribution of conductivity, which means solving the inverse problem. The most common method is Gaussian-Newton(GN) method:

$$\delta\sigma = \boldsymbol{M}\delta U \tag{3}$$

where $\boldsymbol{M}$ represents the linear, one-step reconstruction matrix. It is defined as

$$\boldsymbol{M} = (\boldsymbol{J}^T\boldsymbol{W}\boldsymbol{J} + \lambda^2\boldsymbol{R})^{-1}\boldsymbol{J}^T\boldsymbol{W} \tag{4}$$

In Equation (4), $\boldsymbol{W}$ is the weight of matrix, λ is a regularization parameter chosen heuristically, $\boldsymbol{R}$ is regularization matrix. Based on the finite element method and GN algorithm, we obtained the imaging results of EIT.

The operation of solving inverse problems transforms voltage vectors into images that contain a wealth of meaningful information, especially regarding the spatial structure of conductivity distributions. Compared with raw data and EIT results, more shape and organizational information can be used for training in convolutional neural networks.

Focusing on specific human impedance issues, we employ only a two-terminal scheme [19] with eight electrodes for conducting impedance analysis. As time passed, the arrangement of electrodes may change due to human movement. The possible arrangement have been shown before and after rotation in Figure 3, followed by the collected voltage data V1 and V2 in corresponding electrode arrangement. The difference between V1 and V2 is not significant. However,

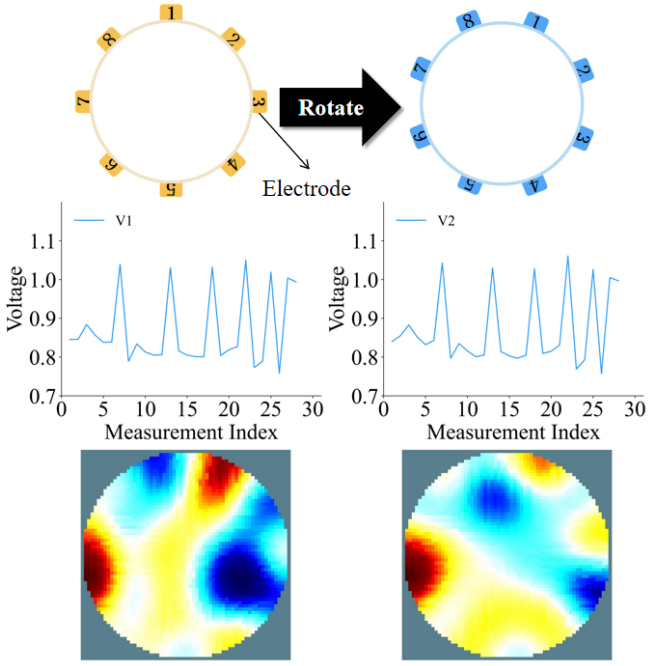

Fig. 3. The image first shows the electrode patterns before and after the offset occurred during the collection time, followed by the voltage data they collected at this moment. The corresponding EIT results are at the end.

EIT is ill-posed which meaning that small voltage data changes on the surface do not necessarily represent that there is little change in the impedance inside the target object. The consequence may lead to judgment errors in practical applications, such as medical image detection errors. To address this issue, quantitative analysis of electrode motion position in the subsequent experimental section will be used to determine whether the proposed network is effective.

C. Classification

The process of classification can be divided into three stages.

•The first stage aims to classify the initially collected voltage data in the source domain. The collected voltage data has 28 feature dimensions. To reduce measurement time and get an acceptable accuracy, we generate a feature subset by computing the variance of each dimension and applying Pearson Correlation to filter irrelevant features. Nextly we use t-distributed stochastic neighbor embedding (t-SNE) [20] to mitigate dimensional collapse. As a result, we can obtain basic classification for the source domain. Evaluation using confusion matrices helps assess the impact of classification operations across different datasets. The time required for this phase is relatively short, approximately 500 ms. This duration is closely related to the size of the training set.

•Complex background noise poses challenges in feature extraction, particularly in accommodating electrode offset. Hence, we have deployed a noise addition mechanism [21] to strengthen the robustness of PDAN in the second stage. The addition of Gaussian noise to the initially voltage data as part of the adversarial network prevents the model

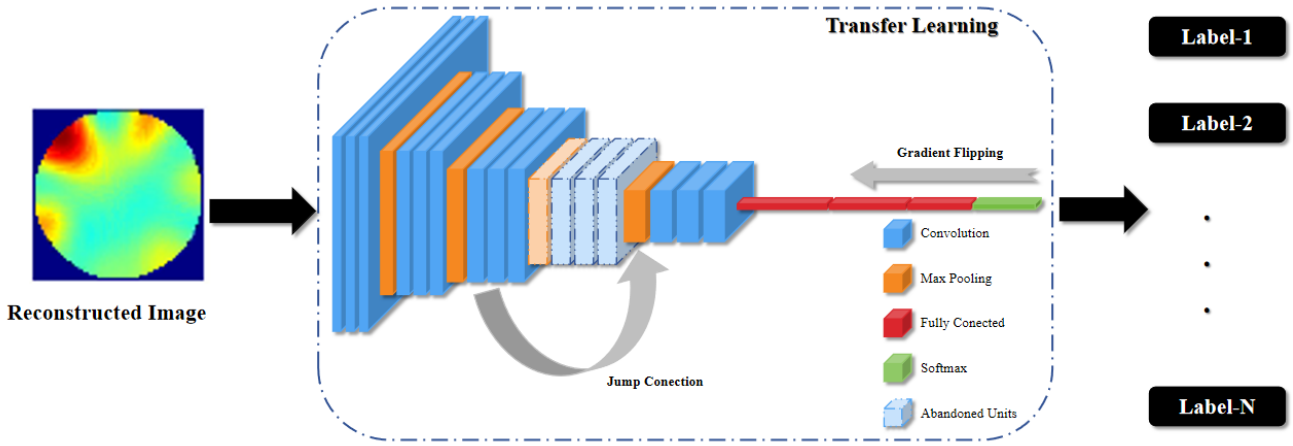

Fig. 4. The PDAN architecture utilizes images as inputs. Employing transfer learning techniques, the network autonomously adjusts various parameters, such as gradient flipping, cross-layer connections, neuron addition, and pruning. This process culminates in the generation of corresponding predicted labels as output results.

from fitting the noise in the collection process. The images with added noise are called ”pseudo-images”, which serve as the dataset for training models to recognize data from the source domain to the target domain. Pseudo-images enable the model to understand electrode rotation operations in real-world significance during the transfer process. The images will be injected into three parallel Conv+ReLU layers. The corresponding outputs are concatenated by four Max pooling layers. Then, attention mechanisms and fully connected layers optimize feature weighting, culminating in enhanced model adaptability. Finally, the softmax function creates a probability distribution matrix, which will output the corresponding maximum probability.

•The final stage involves the process of knowledge transfer shown the main modifications of the entire network in Fig.4. A fine-tuning mode was applied during the adaption of a pre-trained network (Vgg16) model. The feature maps was used from coarse-graining through transfer learning. We adjusted the output category optimization of the last layer of the VGG model for knowledge fine-tuning. The addition of attention mechanism enables the network to annotate the importance of different features. It applies element-wise product between the attention map and the source feature map to increase the weight of pose features. The attention mechanism was embed into the network model to adaptively add or remove neurons. Besides, skip connections and adaptive aggregation mechanisms have also been applied to trim larger network areas. Instead of setting the levels and parameter settings of the convolutional neural network, we utilize domain loss to enable the network to autonomously select parameters. It allows the network to automatically generate convolutional features during forward and backward propagation.

We collected datasets of different leg postures in two states: before and after electrode rotation. The dataset from the former state was used for training, while the latter for testing. In the context of applying EIT to human body, we use pseudo-images to simulate noise [22] and variations in real-world images, by adjusting the recognition of pseudo-images by the label classifier and the domain classifier to minimize the error function, thereby enhancing the model’s adaptability to different data distributions and noise conditions. We call the domain composed of pseudo-images a ”pseudo-domain” and convert the traditional binary domain classifier into a ternary classifier, which is a significant feature of our designed PDAN. Traditional transfer learning is merely a simple adversarial interaction, typically utilizing data under ideal conditions. In the context of human body impedance analysis, we use a pseudo-domain to simulate noise and variations in real-world images, by adjusting the recognition of ”pseudo-images” by the label classifier and the domain classifier to minimize the error function. It helps the model more easily avoid problems of similarity between some original and target domain data caused by system errors, thereby better resisting interference in the target domain.

In the actual process of training transfer, the more data available, the better the model can understand different postures, and the better the results. However, there is a lack of publicly available datasets in the research of this paper. To conduct experiments, we had to create our own dataset. The process of creating a dataset is tedious, and the resources required to add labels are complex. Therefore, we incorporated methods of data augmentation, comparing pixel-level contrasts in the image domain. The strategies employed include random cropping, flipping, and color distortion. Through these means, we can expand from a limited dataset to the required amount, increasing the diversity and complexity of the data. Furthermore, this approach addresses the scarcity and incompleteness of data in the real world, which can help us better learn features and construct the feature space for leg posture classification tasks, thereby improving the model’s generalization capability and robustness.

By incorporating Gaussian noise to introduce pseudo-images, forming a pseudo-domain, and employing data augmentation techniques, we increased data diversity. This helps

to address the issue of data distribution differences between the source and target domains in transfer learning. These improvements bolster the model's adaptability and robustness in transfer learning scenarios.

III. Experiment

A. Leg Posture Set

Displayed in Fig. 5, three types of movements will be tested. Throughout the entire experimental process, the participant will sit on a comfortable chair. Placing the lower leg in its natural resting position is labeled as "relaxed"; slightly lifting the lower leg to half knee height is labeled as "lifted"; crossing the legs with one leg placed above the other thigh is labeled as "crossed legs".

(a) Relax (b) Lift (c) Cross-legged

Fig. 5. Test Motions

We utilized the acquisition system mentioned to record the dataset, obtaining impedance imaging images of the participant in different leg positions (relaxed, lift, crossed-legged), capturing the distribution of internal conductivity in the participant's legs.

TABLE I
Initial and Expanded Datasets Obtained from the Participant

	Relax	Lift	Cross-legged
Original Training Set	200	200	200
Original Test Set	200	200	200
Dataset with Data Enhancement	400	400	400
Dataset with Gaussian Noise	2000	2000	2000

The dataset shown in Table I mainly comes from four aspects:

(1) Original Training Set: The dataset is collected without electrode deviation. A participant keeps their legs still, assuming the Relax, Lift, and Cross-legged postures respectively, and then collects 200 sets of data for each posture.

(2) Original Test Set: The dataset is collected after electrode deviation. A participant remain still, and then the alligator clip is removed. The electrode is moved clockwise by one position and then reconnected. 200 sets of data are collected for each posture.

(3) Dataset with Data Enhancement: The dataset is expanded after data augmentation. Based on the previous two datasets, we applied different data augmentation techniques

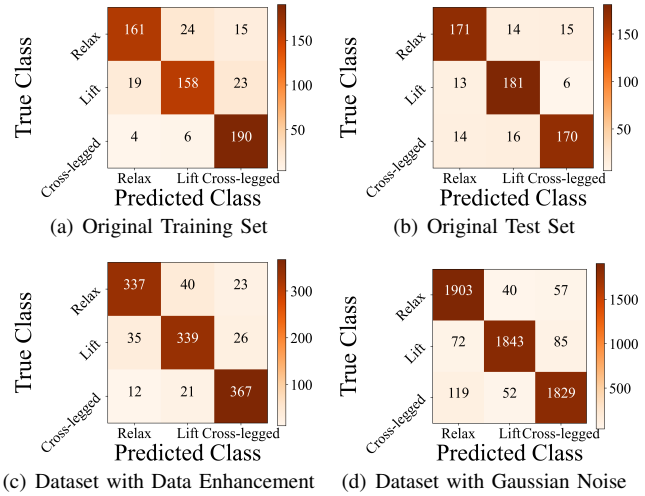

(a) Original Training Set (b) Original Test Set

(c) Dataset with Data Enhancement (d) Dataset with Gaussian Noise

Fig. 6. Confusion matrix for: (a) Training using the training dataset. (b) Training using the original test dataset. (c) Training using the data enhancement dataset. (d) Training using the Gaussian noise dataset.

(flipping horizontally and vertically at four angles, rotation, and zooming) to generate more samples, doubling the dataset.

(4) Dataset with Gaussian Noise: The dataset is simulated with added noise after deviation [23]. Gaussian noise is added to the Training Set and Test Set to simulate changes in data during deviation. This process increases the amount of data 10 times.

B. Basic Setings

All training is conducted on a server with the following configuration: Intel (R) Xeon (R) CPU E5-4600 v4 (4 cores) @2.20GHz, Windows Server 2012 R2 operating system, 112.GB RAM, and PERC H330 Adapter. The input images are converted into three convolutional layers according to the RGB channels. Each layer performs feature calculation using a 3×3 convolutional kernel, effectively extracting structural and textural features from the images. Batch normalization and rectified linear units are applied after each layer, and the size of the feature maps is reduced using a 2×2 pooling window. Finally, three fully connected layers map the high-order features extracted by the convolutional layers to the final output class space, and classification is performed using the Softmax function. The learning rate for all layers is fixed at 0.0001, the maximum batch size is 32, and the weight decay is 0.0001.

C. Result

Applying the previously trained model for classification, confusion matrices were obtained on four datasets, as shown in Figure 6. Rows represent the true categories, while columns represent the categories predicted by the model. The performance difference of PDAN on different datasets is not significant, which proves its universality in different scenarios. Therefore, we will start testing on the fused dataset and compare the performance of PDAN and other common transfer learning methods on all datasets.

(1) Fine-Tuning: Utilizing a model pretrained on a large dataset, all layers except the final fully connected layer are set to non-trainable. The final fully connected layer is modified to 3 to adapt to the current work [24].

(2) RevGrad: Introducing a reverse gradient domain classifier during training, conducting classification tasks between the source and target domains [25].

(3) DANN: Comprising three structures: feature extractor, domain classifier, and label classifier. The feature extractor aims to learn feature representations, the domain classifier attempts to differentiate between the source and target domains, and the label classifier utilizes the learned feature representations from the feature extractor for classification or regression predictions of the target task. It focuses more on achieving similarity in feature representations between different domains, rather than simply transferring knowledge or features [26].

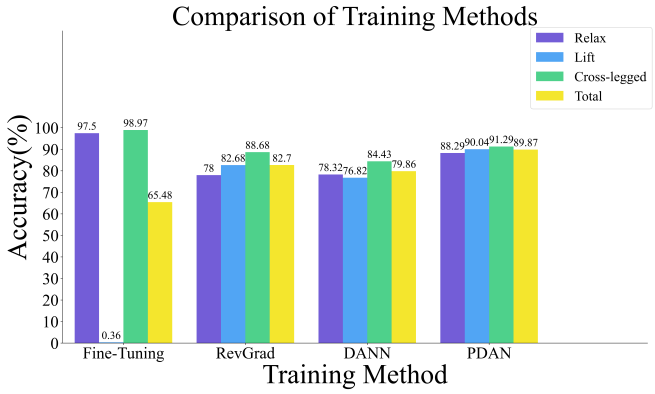

Fig. 7. Comparison of Training Methods

PDAN exhibites the best performance among four methods, reaching nearly 90% accuracy in Fig. 7. It is worth noting that although Fine-Tuning performed well on the action of "relax" and "cross-legged", its overall performance was still poor. We speculate that the poor performance of Fine-Tuning in the second category is due to our use of the voltage data from the "relax" as the baseline for differential imaging. Even slight muscle movements may cause significant changes, making it easier for the model to recognize the images of other poses as the first one. This difference in accuracy may be attributed to the sensitivity of differential imaging, resulting in loss of recognition ability in the "lift" category. Therefore, simple adjustments in the Fine-Tuning method are inadequate for the scenario discussed in this article. Meanwhile, PDAN outperformes RevGra and DANN by nearly 10 percentage points, confirming its efficiency and robustness. The improvement can be attributed to the incorporation of pseudo-domain to simulate electrode rotation, which helps the network understand the process of rotating electrodes.

The network's performance is primarily limited by the acquisition speed of the AD5940 chip. Approximately 350 datasets are collected per minute, which has not yet reached the performance limit of the four comparison networks. Regarding computational costs, PDAN-based architectures include additional components like pseudo domains and attention mechanisms, leading to higher computational requirements compared to simpler models like fine-tuning. However, the performance improvements provided by these additional components justify the increased computational costs in many applications. To emphasize the universality of the model, we further measured the stability of the recall rate at a confidence level of 95%. This level is also the reference value for determining the baseline performance of most current models. With a sample accuracy rate of 0.9017, we can infer with 95% confidence that the model accuracy falls within the range of 87.79% to 92.56%. The model's stability and reliability are confirmed.

IV. Conclusion

In this study, we proposed a pseudo domain adversarial network EIT system with adaptive adjustment to eliminate the impact of human motion on the sliding of wearing device electrodes. Our findings indicate that incorporating a pseudo-domain to simulate electrode rotation significantly improves model performance, achieving nearly 90% accuracy. Moreover, the model exhibits good stability and reliability, with a confidence interval of 87.79% to 92.56% at a 95% confidence level.

These results underscore the potential of our approach in real-world applications, such as monitoring and analyzing human body movements using EIT technology. By addressing challenges such as noise, data distribution differences, and electrode rotation, our model shows promise in enhancing the accuracy and robustness of posture classification systems.

Further research could focus on optimizing model architectures, exploring additional augmentation techniques, and expanding datasets to improve generalization and adaptability. Additionally, real-world validation studies involving diverse populations and conditions would be valuable to validate the scalability and effectiveness of our approach in practical scenarios.

References

[1] Junyi Zhu, Jackson C Snowden, Joshua Verdejo, Emily Chen, Paul Zhang, Hamid Ghaednia, Joseph H Schwab, and Stefanie Mueller. Eit-kit: An electrical impedance tomography toolkit for health and motion sensing. In *The 34th Annual ACM Symposium on User Interface Software and Technology*, pages 400–413, 2021.

[2] L Tarassenko and P Rolfe. Imaging spatial distributions of resistivity-an alternative approach. *Electronics letters*, 14(20):574–576, 1984.

[3] Y Zou and Z Guo. A review of electrical impedance techniques for breast cancer detection. *Medical engineering & physics*, 25(2):79–90, 2003.

[4] Matteo Menolotto, Stefano Rossi, Paolo Dario, and Luigi Della Torre. Towards the development of a wearable electrical impedance tomography system: A study about the suitability of a low power bioimpedance front-end. In *2015 37th Annual International Conference of the IEEE Engineering in Medicine and Biology Society (EMBC)*, pages 3133–3136. IEEE, 2015.

[5] Gang Ma, Zhiliang Hao, Xuan Wu, and Xiaojie Wang. An optimal electrical impedance tomography drive pattern for human-computer interaction applications. *IEEE transactions on biomedical circuits and systems*, 14(3):402–411, 2020.

[6] Wenci Xin, Fangmeng Zhu, Peiyi Wang, Zhexin Xie, Zhiqiang Tang, and Cecilia Laschi. Electrical impedance tomographic shape sensing for soft robots. *IEEE Robotics and Automation Letters*, 8(3):1555–1562, 2023.

[7] ET Hull, T Irie, H Heemstra, and Ch RH Wildevuur. Transthoracic electrical impedance: artifacts associated with electrode movement. *Resuscitation*, 6(2):115–124, 1978.

[8] SC Kim, KC Nam, DW Kim, CY Ryu, YH Kim, and JC Kim. Optimum electrode configuration for detection of arm movement using bio-impedance. *Medical and Biological Engineering and Computing*, 41:141–145, 2003.

[9] A Martínez Olmos, MA Carvajal, DP Morales, A García, and AJ Palma. Development of an electrical capacitance tomography system using four rotating electrodes. *Sensors and Actuators A: Physical*, 148(2):366–375, 2008.

[10] Nobuo Kunori and Ichiro Takashima. A transparent epidural electrode array for use in conjunction with optical imaging. *Journal of neuroscience methods*, 251:130–137, 2015.

[11] Gan Huang, Zhien Xian, Fei Tang, Linling Li, Li Zhang, and Zhiguo Zhang. Low-density surface electromyographic patterns under electrode shift: Characterization and nmf-based classification. *Biomedical Signal Processing and Control*, 59:101890, 2020.

[12] Lizhi Pan, Dingguo Zhang, Ning Jiang, Xinjun Sheng, and Xiangyang Zhu. Improving robustness against electrode shift of high density emg for myoelectric control through common spatial patterns. *Journal of neuroengineering and rehabilitation*, 12(1):1–16, 2015.

[13] Yanyan Shi, Yajun Lou, Meng Wang, Zhiwei Tian, Bin Yang, and Feng Fu. A mismatch correction method for electrode offset in electrical impedance tomography. *IEEE Sensors Journal*, 22(7):7248–7257, 2022.

[14] Giulia Pasquale, Carlo Ciliberto, Lorenzo Rosasco, and Lorenzo Natale. Object identification from few examples by improving the invariance of a deep convolutional neural network. In *2016 IEEE/RSJ international conference on intelligent robots and systems (IROS)*, pages 4904–4911. IEEE, 2016.

[15] Souleyman Chaib, Hongxun Yao, Yanfeng Gu, and Moussa Amrani. Deep feature extraction and combination for remote sensing image classification based on pre-trained cnn models. In *Ninth international conference on digital image processing (ICDIP 2017)*, volume 10420, pages 712–716. SPIE, 2017.

[16] Shaoqing Gao, Shiguang Wen, Chuanjian Ren, Jing Liu, Qi Wu, Lu Han, and Fei Wang. The transfer learning method for reducing the influence of electrode shift. In *2023 IEEE 13th International Conference on CYBER Technology in Automation, Control, and Intelligent Systems (CYBER)*, pages 1241–1246. IEEE, 2023.

[17] Srikanth Tammina. Transfer learning using vgg-16 with deep convolutional neural network for classifying images. *International Journal of Scientific and Research Publications (IJSRP)*, 9(10):143–150, 2019.

[18] Zhangjie Cao, Mingsheng Long, Jianmin Wang, and Michael I Jordan. Partial transfer learning with selective adversarial networks. In *Proceedings of the IEEE conference on computer vision and pattern recognition*, pages 2724–2732, 2018.

[19] Jianjun Chen, Zhang Cao, and Lijun Xu. Four-terminal scheme used in a two-terminal eit system. In *2011 IEEE International Instrumentation and Measurement Technology Conference*, pages 1–5. IEEE, 2011.

[20] Laurens Van der Maaten and Geoffrey Hinton. Visualizing data using t-sne. *Journal of machine learning research*, 9(11), 2008.

[21] Xintong Dong, Ming Cheng, Hongzhou Wang, Guanghui Li, Jun Lin, and Shaoping Lu. A potential solution to insufficient target-domain noise data: Transfer learning and noise modeling. *IEEE Transactions on Geoscience and Remote Sensing*, 2023.

[22] Leila Kiani, Masoud Saeed, and Hossein Nezamabadi-pour. Image colorization using generative adversarial networks and transfer learning. In *2020 International Conference on Machine Vision and Image Processing (MVIP)*, pages 1–6. IEEE, 2020.

[23] Nizar Massouh, Francesca Babiloni, Tatiana Tommasi, Jay Young, Nick Hawes, and Barbara Caputo. Learning deep visual object models from noisy web data: How to make it work. In *2017 IEEE/RSJ International Conference on Intelligent Robots and Systems (IROS)*, pages 5564–5571. IEEE, 2017.

[24] Yunhui Guo, Honghui Shi, Abhishek Kumar, Kristen Grauman, Tajana Rosing, and Rogerio Feris. Spottune: transfer learning through adaptive fine-tuning. In *Proceedings of the IEEE/CVF conference on computer vision and pattern recognition*, pages 4805–4814, 2019.

[25] Zhongyi Pei, Zhangjie Cao, Mingsheng Long, and Jianmin Wang. Multi-adversarial domain adaptation. In *Proceedings of the AAAI conference on artificial intelligence*, volume 32, 2018.

[26] Qikui Zhu, Bo Du, and Pingkun Yan. Boundary-weighted domain adaptive neural network for prostate mr image segmentation. *IEEE transactions on medical imaging*, 39(3):753–763, 2019.